Cross#Equatorial Anti#Symmetry in the Seasonal Transport of the Western Boundary Current in the Atlantic Ocean

manuscripts submitted to *Journal of Geophysical Research – Oceans*

Cross-Equatorial Anti-symmetry in the Seasonal Transport of the Western Boundary Current in the Atlantic Ocean

Yujia Zhai[12], Jiayan Yang[2] and Xiuquan Wan[13]

[1] College of Oceanic and Atmospheric Sciences, Ocean University of China, Qingdao, China, 266100.

[2] Department of Physical Oceanography, Woods Hole Oceanographic Institution, Woods Hole, MA, USA, 02543.

[3] Physical Oceanography Laboratory/CIMST, Ocean University of China and Qingdao National Laboratory for Marine Science and Technology, Qingdao, China, 266100.

Corresponding author: Yujia Zhai (yzhai@stu.ouc.edu.cn) and Xiuquan Wan (xqwan@ouc.edu.cn).

Key Points:

- Equatorial Western Boundary Current seasonal changes are not coherent in tropical Atlantic.
- Zonal symmetric equatorial wind forces the anti-symmetric Equatorial Western Boundary Current seasonal cycle.
- Topography contributes the differences of Equatorial Western Boundary Current between north and south of equator.

Abstract

The western boundary current in the equatorial Atlantic Ocean is a main conduit for water-mass exchanges across the equator and thus a major pathway for the interhemispheric transports in the Atlantic Meridional Overturning Circulation (AMOC) system. In this paper we quantify and examine the mean and seasonal variability of the equatorial western boundary current (EWBC) in the upper ocean layer using two data-assimilated products, the Estimating the Circulation and Climate of the Ocean (ECCO4r3) and the Simple Ocean Data Assimilation (SODA3). It is found that the EWBC between 10°S and 10°N exhibits two pronounced features in its seasonal variability: (1) the transport varies anti-symmetrically across the equator, *i.e.*, the northward EWBC strengthens to the north of the equator when it weakens to the south of the equator, and vice versa; and (2) the amplitude of seasonal variations is much greater in the northern hemisphere than in the south. We hypothesize and test that the cross-equatorial anti-symmetry in EWBC transport variability is attributable to the impingement of equatorial Rossby waves at the western boundary and the shape of the western boundary is the main cause for the amplified seasonal variability in the northern hemisphere. A simple 1 and 1/2 layer model is used to test and validate this hypothesis and to elucidate the role of wind forcing and topography plays in the seasonal variability in the EWBC transport.

Plain Language Summary

The EWBC is the major pathway for transporting water from the South Atlantic to the North Atlantic in the upper ocean layer. Our analyses of two data-assimilated products show that the EWBC transport varies in anti-symmetric phase across the equator, which counters intuition that the EWBC is a continuous and coherent flow. We hypothesize that this anti-symmetry in

EWBC's seasonal variability is attributed to the impingement of equatorial Rossby waves. Long Rossby waves are generated along the equatorial wave guide and propagate westward toward the western boundary. The direction of meridional velocity field induced by an equatorially symmetrical (i.e., odd-numbered meridional mode) Rossby wave is anti-symmetrical across the equator. Upon their impingement at the western boundary, such Rossby waves would result in an anti-symmetrical response in the EWBC transport across the equator. A simple model is used to validate this hypothesis.

1 Introduction

The Atlantic Meridional Overturning Circulation (AMOC) is a key mechanism for the northward heat transport in the ocean and thus an important component in the Earth's climate system. In the upper layer above the main thermocline, the AMOC is responsible for a net northward transport of water mass from the southern to northern hemisphere, primarily along the western boundary. Therefore, the equatorial western boundary current (EWBC) is an important component in the AMOC system and its variability may affect a broad range of oceanic and climate processes. Previous studies have revealed the role of EWBC in the AMOC and in its variability using both observations and model simulations (e.g., Zhang et al., 2011; Rühs et al. 2015). For example, Yang (1999) hypothesized that EWBC variability is linked to the deep-water formation in Labrador Sea. Zhang et al. (2011) showed that the North Brazil Current (NBC hereafter, as the EWBC in the equatorial Atlantic) transport changes at 6°S were significantly correlated with the Atlantic sea surface temperature (SST) and Labrador Sea deep convection on multi-decadal time scales in observations. Furthermore, they suggested that the NBC transport could be considered as an indicator for monitoring the AMOC variations. Other studies have

focused on the pathway of EWBC and its exchanges with interior ocean circulation through selected observational sections (e.g., Schott et al., 1995, 1998, 2002; Bourles et al., 1999; Wienders et al., 2000). Some studies, for instance, analyzed the NBC variations in seasonal and interannual to decadal time-scales, and its role in the AMOC with observations and simulations (e.g., Johns et al., 1998; Zhao and Johns, 2014; Hummels et al., 2015). However, the inter-hemispherical co-variability of EWBC transport remains less studied. Since the EWBC is a main component of the upper AMOC limb, it is important to quantify and understand whether this limb varies coherently across the equator as well.

Previous studies of EWBC have mostly focused on describing its flow structures and quantifying its transport and variability at selected sections. In this study we will examine the continuity of the EWBC transport on the seasonal time scale. Specifically, we will examine the continuity of the EWBC transport across the equator. It is found that the phase of the seasonal variability in the EWBC transport is anti-symmetric across the equator, which is rather counter-intuitive from a perception that the upper AMOC limb is a continuous `belt` and thus is expected to change coherently. The main purpose of this study is to quantify and explain this cross-equatorial anti-symmetry in the seasonal EWBC transport.

The overall structure of the upper layer tropical Atlantic circulation system has been discussed in many previous studies (e.g. Schott et al., 1998; Bourlès et al., 1999; Bourles et al. 1999; Stramma and Schott, 1999). In this study we will focus on the EWBC, which mainly consists of the North Brazil Current (NBC) and the North Brazil Undercurrent (NBUC). The NBC flows northward along the east coast of Brazil, and then moves across the equator. da Silveira et al. (1994) analyzed a set of observations from May 4 to July 12, 1986 and found that the NBC was well developed between 10°S and 5°S with an estimated geostrophic transport of about 21 Sv (1 Sv = 10^6 m^3/s) above 1000 m. They also found that the velocity core of the NBC

in this region was located in the subsurface layer. This undercurrent, named the NBUC, has the maximum velocity up to 90 cm/s between σ_θ = 24.5 and 26.8 kg m^{-3} surfaces (Stramma et al., 1995; Schott et al., 1995, 1998). Observations from 2000-2004 showed that the volume transport of NBUC at 5°S above 1100 m was 26.5 ± 3.7 Sv (Schott et al., 2005). So, it is well recognized that the NBUC is a large component of the EWBC in terms of volume transport. The NBUC is included in our calculation of the EWBC transport that will be presented and discussed in the following sections.

The EWBC feeds various different zonal currents over different depth ranges including the Equatorial Undercurrent (EUC), the North Equatorial Countercurrent (NECC), and the North Equatorial Undercurrent (NEUC). The inter-linkages among such various currents lead to the complexity of tropical circulation system in the Atlantic Ocean. In previous studies the seasonal variability of the EWBC transport is often attributed to the water-mass exchanges between the EWBC and those major zonal currents. For instance, the EWBC variability is firstly contributed to the seasonal retroflection of NBC into NECC (Richardson and Walsh, 1986). Meanwhile, a portion of the NBC continues to flow along the coast and enters the Caribbean Seas along with the water from the North Equatorial Current (NEC) (Schott et al., 1995, 1998). Schott et al. (1998) described the overall transport pathways in the tropical Atlantic Ocean and suggested that the seasonal cycle of the cross-equatorial transport associated with the EWBC was influenced by strongly seasonal variations of the NECC. Johns et al. (1998) analyzed the observations around 4°N and found that the NBC transport reached its maximum in June-August to about 36 Sv and its minimum in April-May at nearly 13 Sv (using current-meter data in the upper 800 m).

In a model study Philander and Pacanowski (1986) also found that the retroflection of NBC into NECC happened between June and November, and surface zonal currents were more influenced by wind forcing from east of 30°W. Weisberg and Weingartner (1988) suggested that the enhancement of trade wind in equatorial Atlantic strengthened westward South Equatorial Current (SEC) between 5°S and equator. Schott et al. (1995, 1998) found that the westward SEC supplies NBC in the surface layer between 5°S and equator. Silva et al. (2009) used the Regional Ocean Modeling System (ROMS) simulation between 2005 and 2007 to investigate the relationship between SEC bifurcation and NBUC transport. They found that stronger northward NBUC transport happened with the southernmost position SEC bifurcation during May 2006 and May 2007, while a minimum northward NBUC transport happened with lower latitude position SEC bifurcation in December 2005 and October-December 2006. In this study, we propose that the equatorial waves play a leading role for the seasonal variability of the EWBC transport. It is important to note that this hypothesis is not contradictory to most previous studies that emphasize the importance of EWBC exchanges with zonal currents. For instance, Busalacchi and Picaut (1983) and Yang and Joyce (2006) demonstrated that the seasonal variability of equatorial zonal currents, such as the NECC, was primarily driven by equatorial waves instead of the local forcing. It is therefore reasonable to extrapolate that a close relationship between EWBC's and NECC's seasonal changes as reported in the aforementioned literatures may be at least partly due to their mutual responses to equatorial forcing instead of a direct forcing of NECC on EWBC.

In next section we will briefly describe the sources of data used in this study, our analysis methodology and a simple 1 and 1/2 layer wind driven model. This will be followed by a discussion of our analyses and modeling results in section 3. A further discussion of forcing mechanisms and a summary will be provided in section 4.

2 Methodology and Data Sources

In an effort to estimate the latitudinal co-variability of EWBC and test the reliability of our results, we analyze two sets of data-assimilated simulations to quantify the EWBC transport's seasonal variability. Then, we use a reduced-gravity model to identify and examine mechanisms for such variability. The data-assimilated products used in this study are the ECCO4r3 (Forget et al. 2015; Fukumori et al. 2017), and SODA3 (Carton et al. 2018; Carton et al. 2019). ECCO4r3 and SODA3 assimilate similar types of observations, such as sea surface height (SSH) from satellite altimeters and *in situ* hydrographic data, etc. The assimilation methodologies are very different in these two products. The cross-comparison of EWBC variability from these two products that use different data assimilation methodologies would enhance the robustness of our analyses and conclusion. For a better comparison, we also choose the products with the same resolution. In addition, a simple 1 and 1/2 layer nonlinear reduced-gravity model is set up for sensitivity experiments.

2.1 ECCO4r3

ECCO4 is a multi-decadal estimate of the state of the global ocean, including the Arctic Ocean (Fukumori et al. 2017). It is based on the MIT General Circulation Model (MITgcm) and assimilates most available modern observations, including sea level height from altimetry, bottom pressure from GRACE and hydrography from Argo profilers. In this study we use the interpolated monthly product from the third release of ECCO4 between 1992 and 2015

(ftp://ecco.jpl.nasa.gov/Version4/Release3/). The gridded ECCO4r3 fields have the same horizontal resolution with SODA3.4.2 (1/2°×1/2°) and 50 vertical levels.

2.2 SODA3.4.2

SODA3.4.2 is a new generation of the SODA products, which is a data-assimilated simulation based on the Modular Ocean Model version 5.1 (MOM5.1) and forced by ERA-Interim (Dee et al. 2011), a global atmospheric reanalysis and used COARE4 (Coupled Ocean Atmosphere Response Experiment) bulk formula (Carton et al. 2018). This dataset covers the time period from 1980 to 2018 (https://www.atmos.umd.edu/~ocean/index.htm). We use the monthly mean climatology with a 1/2°×1/2° Mercator horizontal grid and a 50-levels vertical grid (the vertical resolution is about 10 m in the upper 100 m).

3 EWBC and tropical circulation in ECCO4 and SODA

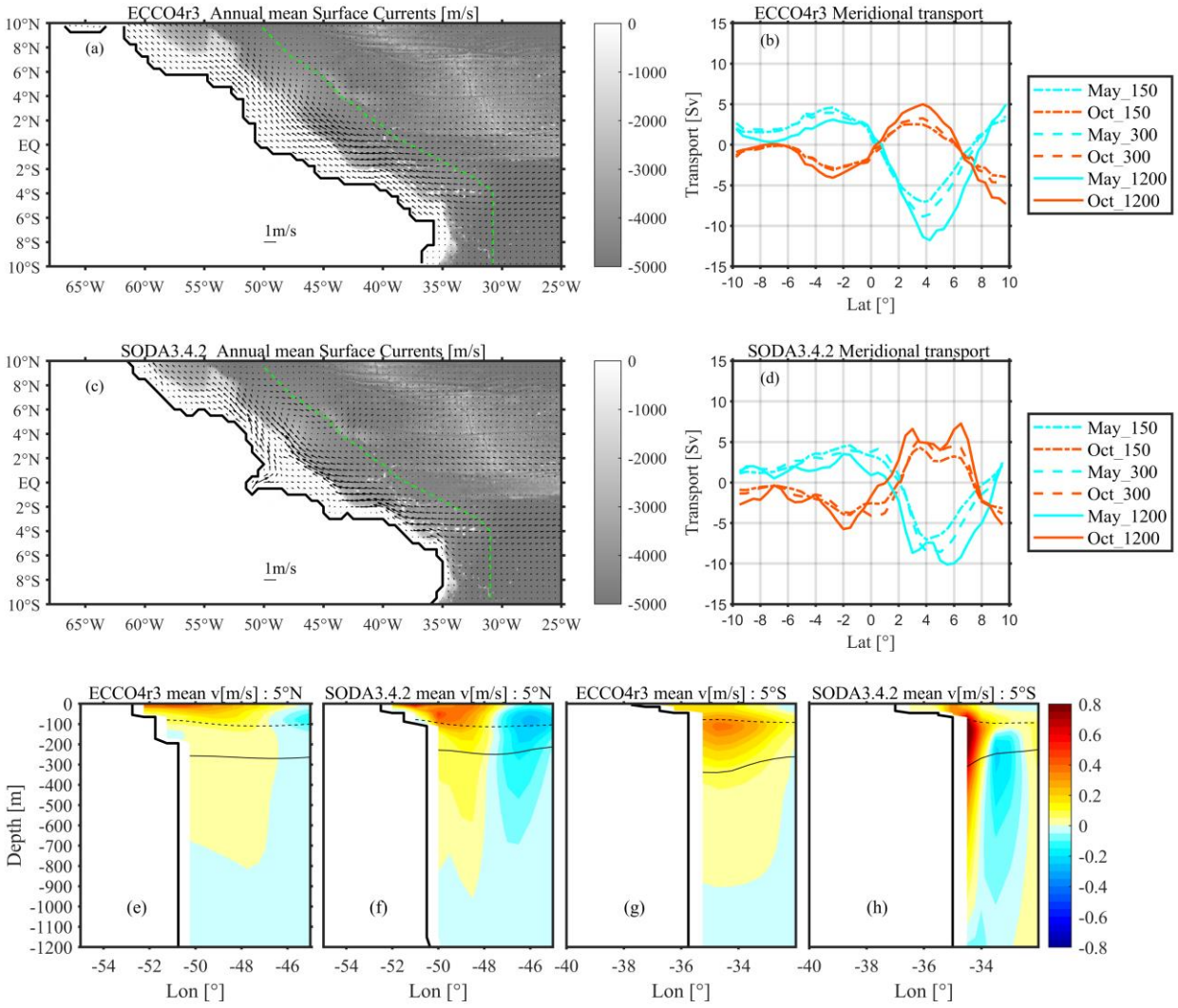

Figure 1. (a) ECCO4r3 annual mean sea surface currents (vectors) in western equatorial Atlantic with topography in color (green dashed line marks the offshore edge of EWBC); (b) ECCO4r3 monthly anomalies of the northward EWBC transport in May (blue lines) and October (red lines) on different depth ranges (from surface to 150 m/ 300 m/ 1200 m with individual line style); (c)-(d) same as (a)-(b) except for SODA3.4.2 product; (e) ECCO4r3 annual mean meridional velocities at 5°N (the black dashed line marks the isopycnal surface $\boldsymbol{\sigma_\theta = 24.5\ kg/m^3}$**;** the

black solid line marks the isopycnal $\boldsymbol{\sigma_\theta = 26.8\ kg/m^3}$); (f) same as (e) except for SODA3.4.2 product; (g)-(h) same as (e)-(f) except for 5°S.

Here we use the annual-mean sea surface current to define the EWBC as the flow from the coast to an offshore position where the mean northward intensified boundary flow diminishes, which is marked by the green lines in Figure 1a and 1c for ECCO4 and SODA respectively. The EWBC south of 5°S has a narrower width than that to the north of equator (the topography in Figure 1a and 1c from ETOPO1 (Amante and Eakins, 2009)). There are some noticeable differences in the coastlines in ECCO4 and SODA as shown in Figure 1 and the differences are due to the use of different land mask grids in these two products. The overall impact of land-mask discrepancy on the integrated transports is likely to be very small because the land-mask differences occur mostly on grids along the coastline where the water depth is near zero.

We will present two sets of the EWBC transport, one based on depth coordinate and the other on the potential density coordinate. In the first set of calculations, the EWBC transport at each latitude is computed by integrating the transport vertically from the surface to a prescribed depth level between the coast and the green lines in Figure 1a and 1c. Since we are primarily interested in monthly anomalies, the annual-mean transport is removed in the following analyses. Figure 1b and 1d show the seasonal anomaly of the EWBC transport in May (blue lines) and October (red lines) from 10°S to 10°N from ECCO4 (upper right panel) and SODA (lower right panel) products respectively. Three depth levels are used in the vertical integration, 150m, 300m and 1200m. The magnitude of the transport anomaly increases with the depth of integration, indicating that the velocity in the upper 1200 m is generally in the same direction along the western boundary. The overall spatiotemporal patterns of the transport anomaly, however, remain qualitatively the same for transports using the three different integration depths. The most

noticeable feature in Figure 1b and 1d is that the seasonal anomaly of the EWBC transport is anti-symmetrical about the equator. In October, for instance, the transport is anomalously high in the northern hemisphere but is low to south of the equator. The same anti-symmetrical feature is also evident in May when the transport anomaly pattern reverses. It is interesting to note that this anti-symmetry feature is evident in both ECCO4 and SODA products, indicating that this feature is not model dependent. It is also worth noting that the amplitude of the seasonal transport anomaly is comparable for both products. Another noticeable feature in Figure 1b and 1d is that the amplitude of the seasonal anomaly in the EWBC transport is much greater in the northern hemisphere than that in the southern hemisphere. We postulate that this northern enhancement pattern is mainly due to the shape of the coastline. It will be investigated further with 1 and 1/2 layer model simulations. Figure 1 e-h show the vertical distribution of meridional velocities at 5°N and 5°S in ECCO4 and SODA, respectively. Comparing with the distribution at 5°N, the core of meridional velocities at 5°S is located in the subsurface layer between σ_θ = 24.5 and 26.8 kg m^{-3} surfaces both in ECCO4 and SODA, which is consistent with available observations discussed previously. However, the width of EWBC in ECCO4 is larger than that in SODA with the smaller maximum velocities. The discrepancy may be partly due to the difference in model setups like spatial resolutions.

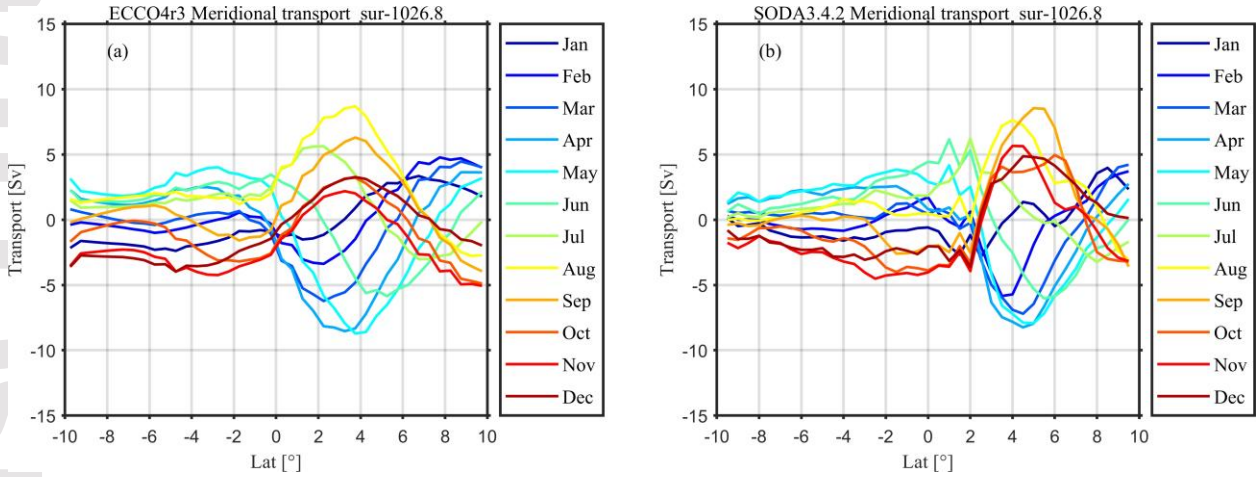

Figure 2. (a) Monthly anomaly of the EWBC transport of water mass $\boldsymbol{\sigma_\theta \leq 26.8\ kg/m^3}$ from ECCO4r3; (b) same as (a) except for SODA3.4.2.

Our second method in computing the EWBC transport is based on the potential density coordinate. Following previous studies (Stramma et al., 1995; Schott et al., 1995, 1998), the EWBC transport is defined as the vertically-integrated transport from the sea surface to the isopycnal surface of $\sigma_\theta = 26.8\ kg/m^3$. We use the Gibbs Sea Water (GSW) Oceanographic Toolbox (McDougall and Barker, 2011) of TEOS-10 to calculate the potential density from salinity and potential temperature. The monthly anomaly of the EWBC transport is shown in Figure 2 (left panel for ECCO4 and the right for SODA). The hemispherical anti-symmetry in EWBC transport anomaly is very similar to that shown in Figure 1. This feature is very robust for all 12 months through the annual cycle. Figure 2a and 2b show that the EWBC transport south of the equator is high during April-June and low in other months, while the EWBC north of equator is low during April-June and high in other months. Johns et al. (1998) showed the seasonal cycle of NBC around 4°N from surface to 800 m. While their observational section was not an exactly zonal section as that shown in Figure 1 and 2, they showed that the transport was indeed low during April-May, which is consistent with our analyses of ECCO4 and SODA.

Figure 2 also reveals that the amplitude of seasonal anomaly in EWBC transport is larger north of the equator than that south of equator – the same as that shown in Figure 1. Despite a good overall agreement between two products, there are some noticeable differences. For example, the transport reverses its phase nearly the equator in ECCO4, while nearly 2°N in SODA; the amplitude of transport variability south of the equator is larger between 4°S and 2°S in ECCO4, but it is larger between 2°S and equator in SODA; the transport between the equator and 6°N in ECCO4 keeps the maximum value in August, while it swings between August and September in SODA.

Figure 3 shows the May and October anomalous thickness between sea surface and $\sigma_\theta = 26.8\ kg/m^3$ surface and the depth-averaged velocity from ECCO4 (upper 2 panels) and SODA (lower two panels). Near the western boundary the isopycnal surface shallows in May, which results in an equatorward velocity anomaly between 6°S and 6°N. In October, the along boundary velocity is reversed to the poleward direction. Figure 4 shows the anomalous thickness between sea surface and $\sigma_\theta = 26.8\ kg/m^3$ surface at both 3°N and 3°S from ECCO4 (Figure 4a and 4c) and SODA (Figure 4e and 4g). The significant seasonal signals are symmetrical at 3°N and 3°S and propagate westward from eastern equatorial Atlantic. Correspondingly, Figure 4 shows the monthly anomaly of the EWBC transport of between sea surface and $\boldsymbol{\sigma_\theta = 26.8\ kg/m^3}$ surface at both 3°N and 3°S from ECCO4 (Figure 4b and 4d) and SODA (Figure 4f and 4h). However, the seasonal variations of EWBC transport changes anti-symmetrically at 3°N and 3°S both from ECCO4 and SODA. Furthermore, the amplitude of EWBC transport seasonal variations at 3°N is much larger than 3°S both in ECCO4 and SODA. The dynamic

process will be examined in the later sections.

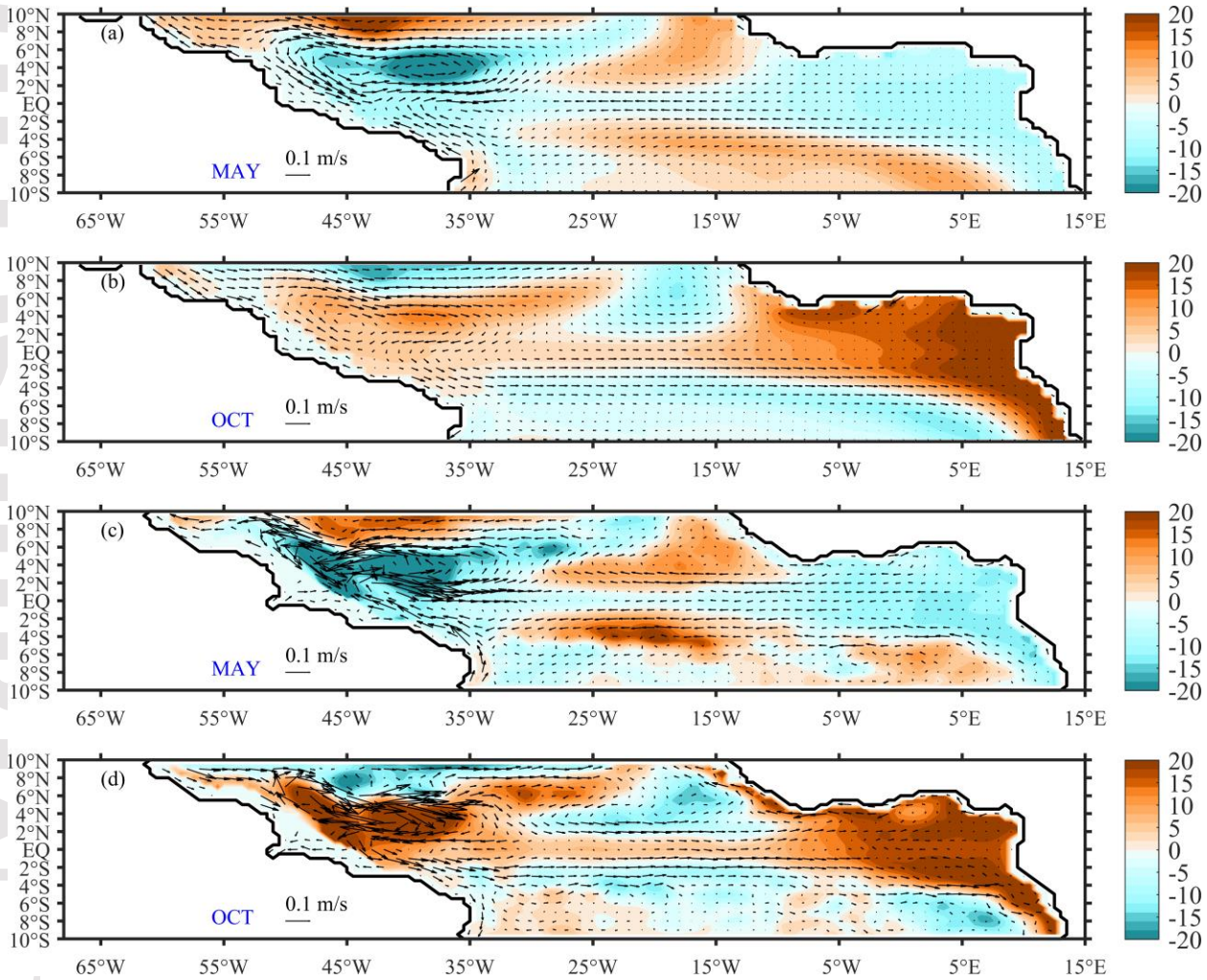

Figure 3. (a)-(b) Thickness anomalies [m] of between sea surface and $\boldsymbol{\sigma_\theta = 26.8\ kg/m^3}$ isopycnal surface (color) and depth-averaged velocity (vectors) between sea surface and $\boldsymbol{\sigma_\theta = 26.8\ kg/m^3}$ surface in May and October from ECCO4r3 data; (c)-(d) same as (a)-(b) except for SODA3.4.2 product.

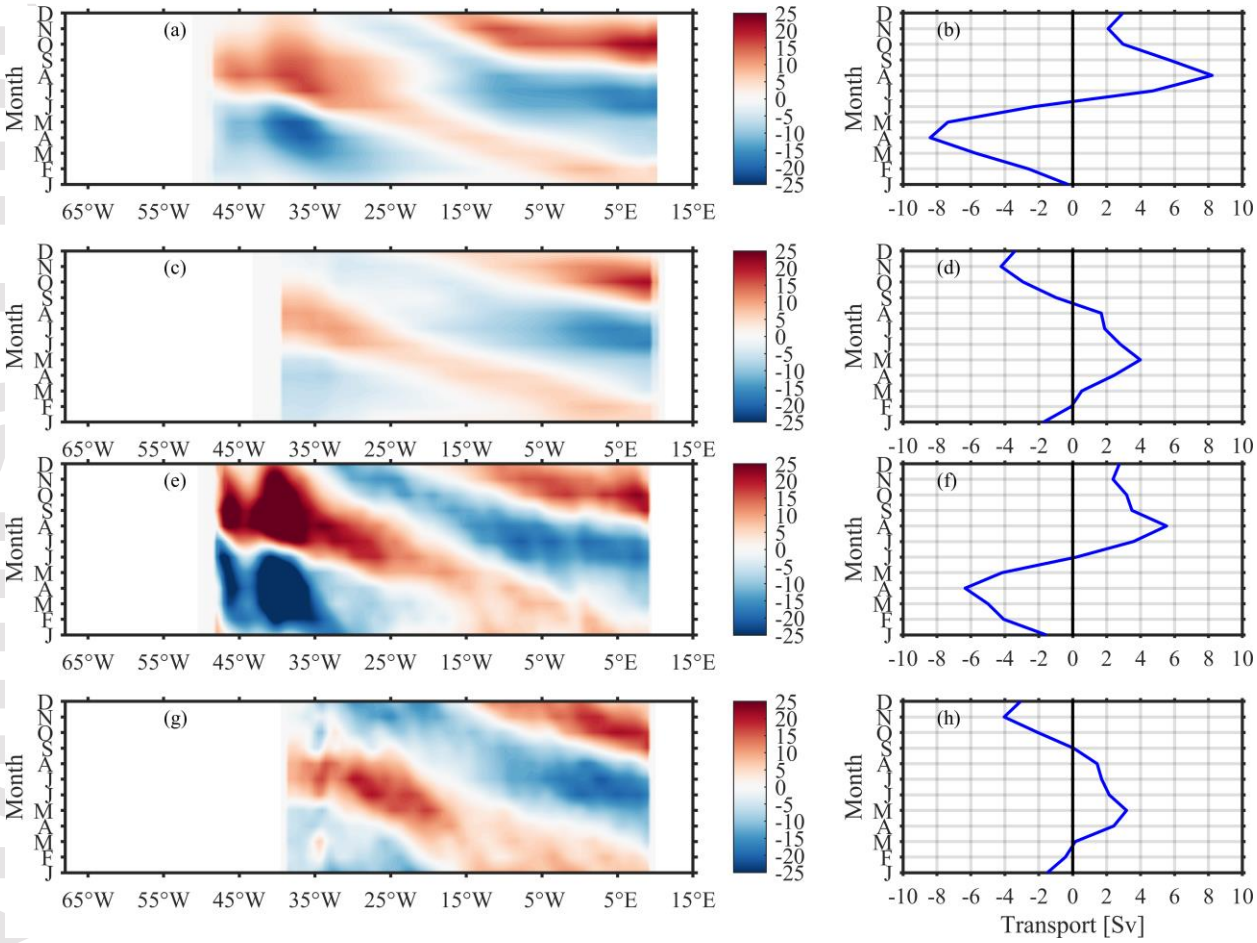

Figure 4. (a) Thickness anomalies [m] of between sea surface and $\boldsymbol{\sigma_\theta = 26.8\ kg/m^3}$ isopycnal surface (color) at 3°N; (b) Monthly anomaly of the EWBC transport of between sea surface and $\boldsymbol{\sigma_\theta = 26.8\ kg/m^3}$ surface at 3°N from ECCO4r3 data; (c)-(d) same as (a)-(b) except for results at 3°S from ECCO4r3 data; (e)-(h) same as (a)-(d) except for SODA3.4.2.

From the analyses of Figure 3 and 4, we hypothesize that the anti-symmetry of the seasonal transport in EWBC is attributable to the impingement of westward propagating equatorial Rossby waves, and the disparity in the amplitude of seasonal variability across the equator is influenced by the shape of the western boundary. A simple 1 and 1/2 layer reduced-gravity model is used here to test our hypothesis. The model is basically the same as that used by Yang and Joyce (2006). It simulates the variability of the upper layer thickness and velocity

field. We choose properly the model parameter $\Delta\rho$ so that the model layer interface represents the surface of $\sigma_\theta = 26.8\ kg/m^3$.

4 One and a half layer nonlinear Model

We use a simple 1 and 1/2 layer reduced-gravity model (Yang and Joyce, 2006) in our mechanism study. The model is governed by the following equations:

$$\frac{\partial u}{\partial t} + u\frac{\partial u}{\partial x} + v\frac{\partial u}{\partial y} - fv + g'\frac{\partial H}{\partial x} = A_H\nabla^2 u + \frac{\tau^x}{\rho H},$$

$$\frac{\partial v}{\partial t} + u\frac{\partial v}{\partial x} + v\frac{\partial v}{\partial y} + fu + g'\frac{\partial H}{\partial y} = A_H\nabla^2 v + \frac{\tau^y}{\rho H}, \quad (1)$$

$$\frac{\partial h}{\partial t} + \left(\frac{\partial (Hu)}{\partial x} + \frac{\partial (Hv)}{\partial y}\right) = 0.$$

The model uses the spherical coordinate with a resolution of 0.25° both zonally and meridionally and is integrated from an initial condition of rest with *H=150m*. We use $A_H = 2500\ m^2 s^{-1}$ for the model viscosity, which yields the Munk WBC width, $L_M = (A_H/\beta)^{1/3}$, about 50km. Previous studies suggested that the second baroclinic mode was dominant in the seasonal cycle of sea level in the tropical Atlantic Ocean (e. g. Busalucchi and Picaut, 1983; McCreary et al., 1984; Yang and Joyce, 2006). So, we choose the reduced gravity *g'* so that the shallow-water gravity wave speed holds to be $c = \sqrt{g'H} = 1.3\ ms^{-1}$. The boundary conditions are closed with condition of no-normal flow and no-slip. Our model domain is from 100°W to 20°E zonally and from 40°S to 40°N meridionally. We use the wind stress data from the Objectively Analyzed air-sea Fluxes (OAFlux) (Yu and Jin, 2010) in Eq. (1). We choose the monthly mean climatology (1993-2015) for running model with a horizontal resolution of 1/4°×1/4°.

We design a series of experiments to investigate the seasonal cycle of EWBC (see Table 1 for the list of experiments). First, we conduct a `control-run` simulation using the forcing over the whole model domain. Figure 5a shows the mean currents of western tropical Atlantic in the control run, and the red dashed line indicates the offshore edge of the EWBC. It should be pointed out that the reduced-gravity model assumes a flat bottom and therefore there is no topographic effects on the model flow field. It is also important to point out that the 1 and 1/2 layer model is forced by wind stress alone and so there is no mean overturning circulation. The western boundary current north of 6°N is southward. This is in contrast with a continuous northward flow in the ECCO4 and SODA, which is attributed to a net northward transport associated with AMOC's upper limb. The seasonal variability with the annual-mean removed, however, is more comparable with that from data-assimilated products.

The monthly variability of the EWBC transport anomaly from the 1 and 1/2 layer model, shown in Figure 5b is qualitatively similar to that from ECCO4 and SODA (Figure 2). The two features that we seek to explain, i.e., the transport anomaly is anti-symmetrical about the equator and the amplitude of the transport anomaly is much greater north of the equator, are simulated well in this control run. Similar to that from ECCO4 and SODA, the EWBC transport in April-June is weak north of equator and strong south of equator, and vice versa for the fall season. The model-simulated seasonal deviations of layer thickness and velocity, shown in Figure 5c and 5d, are similar qualitatively with that from ECCO4 and SODA (Figure 3). Despite the similarity that the maximum northern EWBC transport occurs in August/September, which is the same as that in ECCO4 and SODA, the transport in 1 and 1/2 layer model decreases more rapidly toward the end of the year than that in two data-assimilated datasets. The seasonal changes of layer thickness and EWBC transport at 3°N and 3°S are shown in Figure 5e-5h which are similar with

both ECCO4 and SODA shown in Figure 4. The consistency in the seasonal anomaly of the EWBC transport between the 1 and 1/2 layer model and both ECCO4 and SODA indicates that the model is suitable for identifying and examining leading mechanisms that are responsible for the two features identified in analyses of ECCO4 and SODA, i.e., the equatorial anti-symmetry in EWBC transport anomaly and the enhancement of seasonal transport variability north of the equator.

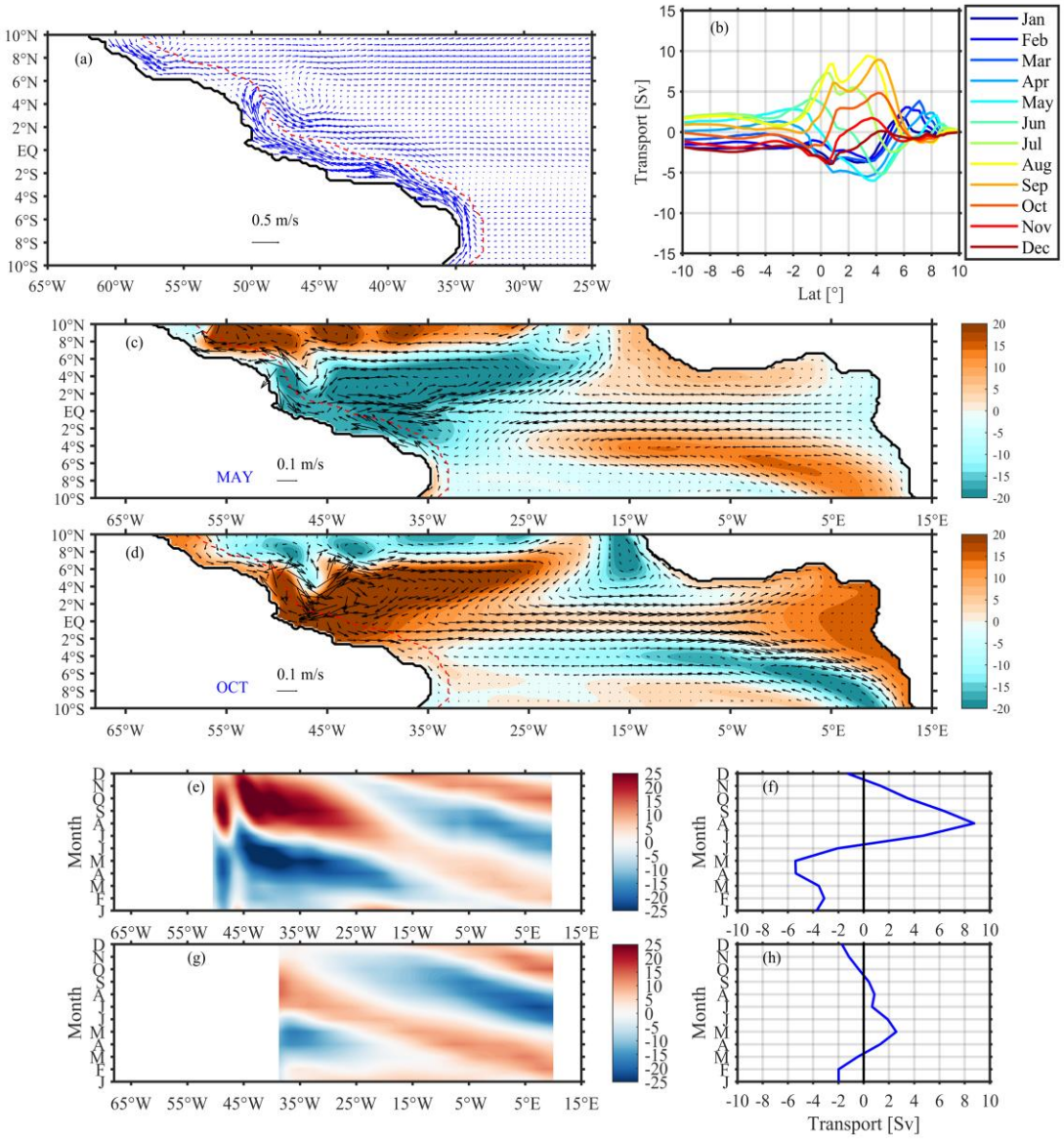

Figure 5. (a) Annual mean velocity from the control run; (b) Monthly anomalies of the EWBC transport in control run; (c) Monthly anomalies of layer thickness [m] and velocity in May; (d) Monthly anomalies of layer thickness [m] and velocity in October; (e) Monthly anomalies of layer thickness [m] at 3°N; (f) Monthly anomalies of the EWBC transport at 3°N; (g)-(h) same as (e)-(f) except for 3°S.

Table 1. Equatorial wind Experiments configuration

M1	Only seasonal equatorial wind (2.5°S-2.5°N)
M2	Only seasonal equatorial wind (2.5°S-2.5°N) between 35°W and east coast
M3	Only seasonal equatorial wind (2.5°S-2.5°N) between west coast and 35°W
M4	Only symmetric seasonal equatorial wind
M5	Only anti-symmetric seasonal equatorial wind

4.1 Equatorial wind experiments

In this section, we use five experiments to examine the role of equatorial wind in modulating EWBC. Results from 5 experiments will be discussed here. In each experiment the annual mean wind stress is applied and the seasonally-varying wind stress is applied only in the equatorial region between 2.5°S and 2.5°N within two zonal dashed lines in Figure 6a. In the first experiment, M1, the seasonal wind stress anomaly is applied from the western to the eastern boundary within this 5° equatorial band. Addition 4 experiments (M2-M5) are conducted in which the seasonal wind-stress anomaly is altered so that different processes/mechanisms can be isolated and examined. The 5 experiments (M1-M5) are listed and explained in Table 1.

In the first equatorial forcing experiment (M1), the seasonally-varying forcing is applied only within the 2.5°S-2.5°N equatorial zone. The EWBC transport shown in Figure 6b, however, closely resembles that from the control run (Figure 5b) in which the seasonally-varying wind stress is applied over the whole model domain from 40°S to 40°N. This similarity indicates that a leading role of wind stress is performed in the equatorial zone for the EWBC variability. The equatorial forcing alone simulates well the two leading features of the EWBC transport variability, i.e., (i) the seasonal transport anomaly is anti-symmetrical about the equator and (ii) the amplitude of change is much greater in the northern hemisphere.

Next, we will examine whether the shapes of coastlines affect the any of these two features. Within the 2.5°S-2.5°N equatorial belt, it appears that the western boundary is more slanted than the eastern boundary. Slanted boundaries lead to meridional anti-symmetries in momentum flux to the ocean between the northern and southern equatorial ocean, and also affect reflections of equatorial waves at boundaries. The goal of the next two experiments, M2 and M3, is to examine how the shapes of coastline at the eastern and western boundaries affect the seasonal variability of the EWBC transport. In experiment M2 the model is forced by wind stress only to the east of 35°W and within 2.5°S-2.5°N region so the shape of western boundary does not contribute to differences in momentum flux between the northern and southern equatorial ocean. Figure 6c shows that the seasonal transport anomaly is anti-symmetrical about the equator but the amplitude of the seasonal variability is comparable between the northern and southern hemisphere. The result from M2 indicates that the shape of the western boundary is not responsible for the cross-equator anti-symmetry in EWBC transport but may be important for the enhancement of the transport north of the equator. In the follow-on experiment M3, the model is forced by the equatorial wind stress between the western boundary and 35°W. The EWBC

transport (Figure 6d) shows that the seasonal variability of the EWBC transport is small in the southern hemisphere. The seasonal variability is predominantly in the northern hemisphere. Together with the previous experiment (M2), it becomes obvious that it's the shape of the western boundary that is most likely responsible for the high amplitude of seasonal variability in the EWBC transport north of the equator.

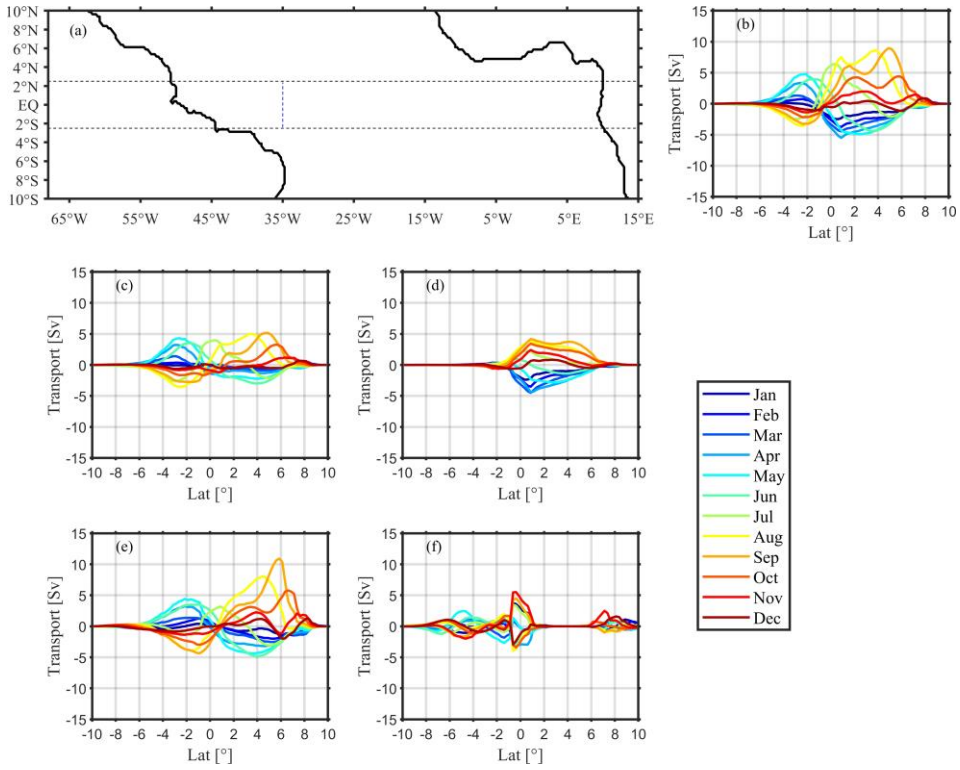

Figure 6. (a) Equatorial forcing area as indicated by dashed lines (the short dashed-line is at 35°W). Five experiments are conducted with equatorial forcing as listed in Table 1. (b)-(f): monthly EWBC transport anomalies for experiments M1-M5.

There are primarily two types of equatorial waves that are relevant at the seasonal time scale, eastward Kelvin waves and westward Rossby waves. From the monthly anomalies of layer thickness at 3°N and 3°S, it is clear that the signal propagates westward. So, for the EWBC it is the Equatorial Rossby waves that we need to consider. For equatorial Rossby waves, there are

infinite number of meridional modes that are associated with each vertical mode. The odd-numbered meridional modes are symmetrical about the equator while the even-numbered modes are anti-symmetrical across the equator (Gill, 1980). For an existing northward EWBC, the impingement of a symmetrical Rossby wave (odd-numbered mode) at the western boundary would result in an equatorially anti-symmetrical response in the EWBC transport, and the reflection of anti-symmetrical Rossby wave leads a symmetrical response in the EWBC. This mechanism is schematized in Figure 7.

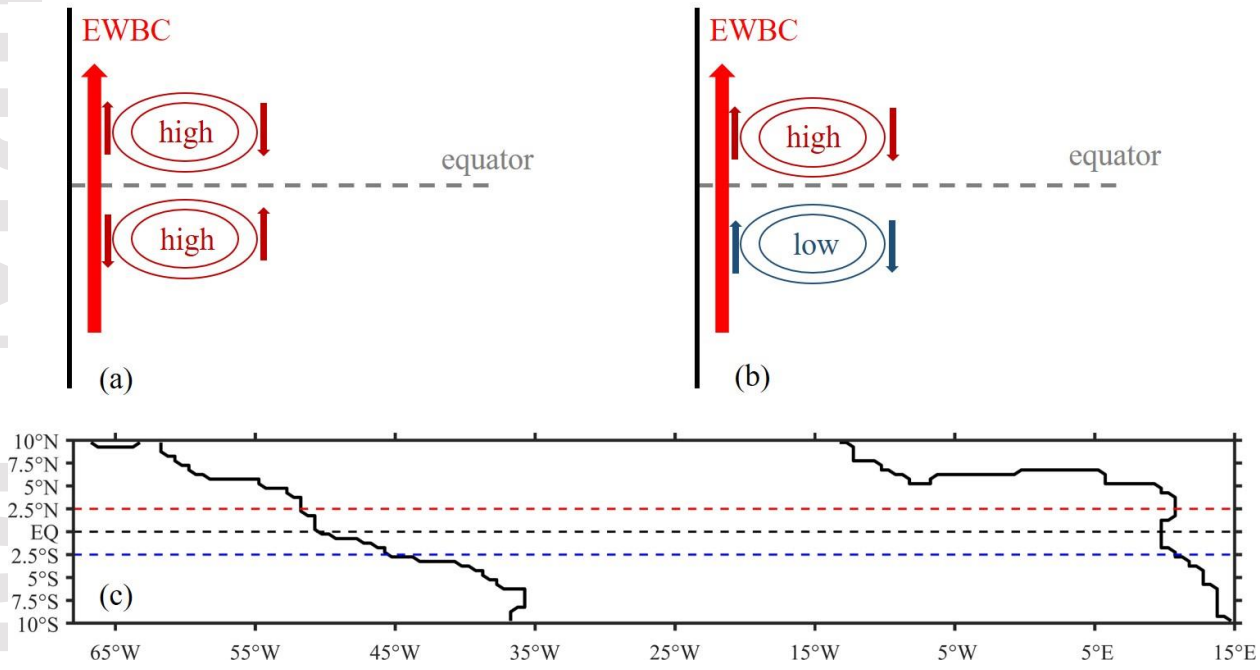

Figure 7. Schematic of how the impingement of a symmetrical Rossby wave (a) and an anti-symmetrical Rossby wave (b) at the western boundary affects the EWBC transport. A symmetrical Rossby waves (odd-numbered meridional modes) at the western boundary would result in a strengthening (weakening) in the northern and weakening (strengthening) in the southern EWBC, leading to an anti-symmetrical anomaly of EWBC across the equator as shown in the upper left panel. The impact of an anti-symmetrical Rossby wave, however, would result

386 in a simultaneously strengthening or weakening on both sides of the equator as shown in the
387 upper right panel. (c) Coastline of equatorial Atlantic. The black dashed line marks the equator.
388 The blue and red dashed lines mark 2.5°S and 2.5°N. The shape of coastline is the same with
389 ECCO4r3.

390

391 To induce an inter-hemispheric anti-symmetry of a northward EWBC, the meridional
392 velocity anomaly associated with an incident Rossby waves needs to be poleward or equatorward
393 on both sides of the equator simultaneously. Such incident waves would need to be odd-
394 numbered meridional Rossby modes, which are symmetrical about the equator (schematized in
395 Figure 7a). It is obvious that a symmetrical forcing along the equator would likely generate odd-
396 numbered meridional Rossby modes that are symmetrical about the equator, and vice versa for
397 the anti-symmetrical modes (Figure 7b). Here we decompose the equatorial wind stress anomaly
398 to both symmetrical and anti-symmetrical components. The method for decomposition is as
399 follows:

400 $$\vec{\tau'}(x,y,t) = \vec{\tau'}_s(x,y,t) + \vec{\tau'}_a(x,y,t) \quad (2)$$

401 where $\vec{\tau'}_s$ and $\vec{\tau'}_a$ are the equatorially symmetrical and anti-symmetrical components of wind
402 stress anomaly respectively. These two components can be defined as follows:

403 $$\vec{\tau'}_s(x,y,t) = [\vec{\tau'}(x,y,t) + \vec{\tau'}(x,-y,t)]/2 \quad (3)$$

404 $$\vec{\tau'}_a(x,y,t) = [\vec{\tau'}(x,y,t) - \vec{\tau'}(x,-y,t)]/2 \quad (4)$$

There are areas near the western and eastern boundaries where such decomposition cannot be performed because of slanted coastlines. On those small areas the seasonal anomaly of wind stress is set to be zero.

In the next experiment (M4), the model is forced by the annual-mean wind stress over the whole domain plus the symmetrical component of the wind stress anomaly within the 2.5°S-2.5°N. The seasonal anomalies of the EWBC from M4 (Figure 6e) is both qualitatively and quantitatively similar to that of M1 (Figure 6b). This supports our hypothesis that it is the symmetrical Rossby waves that are responsible for the anti-symmetrical anomalies of the seasonal EWBC transport. The result from using anti-symmetrical wind forcing experiment (M5) is shown in Figure 6f. The EWBC response is relatively small except at the equator. From experiments M1-M5, we conclude that (1) the equatorial wind plays the major role for the EWBC anti-symmetric season cycle, especially in 6°S-6°N; and (2) the symmetric equatorial wind makes a great contribution on the anti-symmetric latitudinal differences of EWBC seasonal transport variations.

Table 2. Idealized wind and coastline Experiments configuration

E1	*wind forcing in the box (dashed line box in Figure 8a)*
E2	*same as E1 except replacing the western boundary by a straight lined (red line in Figure 8a)*
E3	*same as E1 except replacing the eastern boundary by a straight lined (blue line in Figure 8a)*
E4	*wind forcing expanded zonally from the western to the eastern boundary within 2.5°S-2.5°N*

4.2 Idealized wind and coastline Experiments

To better understand the role of the slanted coastline on the EWBC transport variability, we decide to conduct a few additional experiments using idealized forcing fields and altered coastlines (see Table 2). The model configuration is consistent with our control run. As we have discussed above, it's the symmetrical component of the zonal wind stress along the equator that plays a leading role in regulating the EWBC's seasonal variability and gives rise to two prominent features that are diagnosed from ECCO4 and SODA. Therefore, we will use a zonal wind stress that is symmetrical about the equator in this set of experiments. The meridional wind stress is assumed zero. The zonal wind stress is prescribed as follows:

$$\tau_x(x,y,t) = \tau_0 * \cos\left(\frac{\pi y}{5^\circ}\right) * \sin\left(\frac{2\pi t}{360 days}\right), \quad (5)$$

The wind is applied only within an equatorial region indicated by the box in Figure 8a (between 35°W and 10°W, between 2.5°S and 2.5°N). There is no forcing outside this area. We use $\tau_0 = -0.01 N/m^2$ in these idealized simulations (τ_0 is comparable with the magnitude of seasonal anomaly of wind stress in this region; the area mean observational wind stress in the same box area is about $-0.03 N/m^2$). The first idealized experiment, E1, is conducted by using the zonal wind stress prescribed in Eq. (5) and the unaltered coastline as in the control run. The result shows an anti-symmetrical anomaly of EWBC seasonal meridional transport across the equator (Figure 8b). The amplitude of the seasonal anomaly, however, is about the same on two sides of the equator.

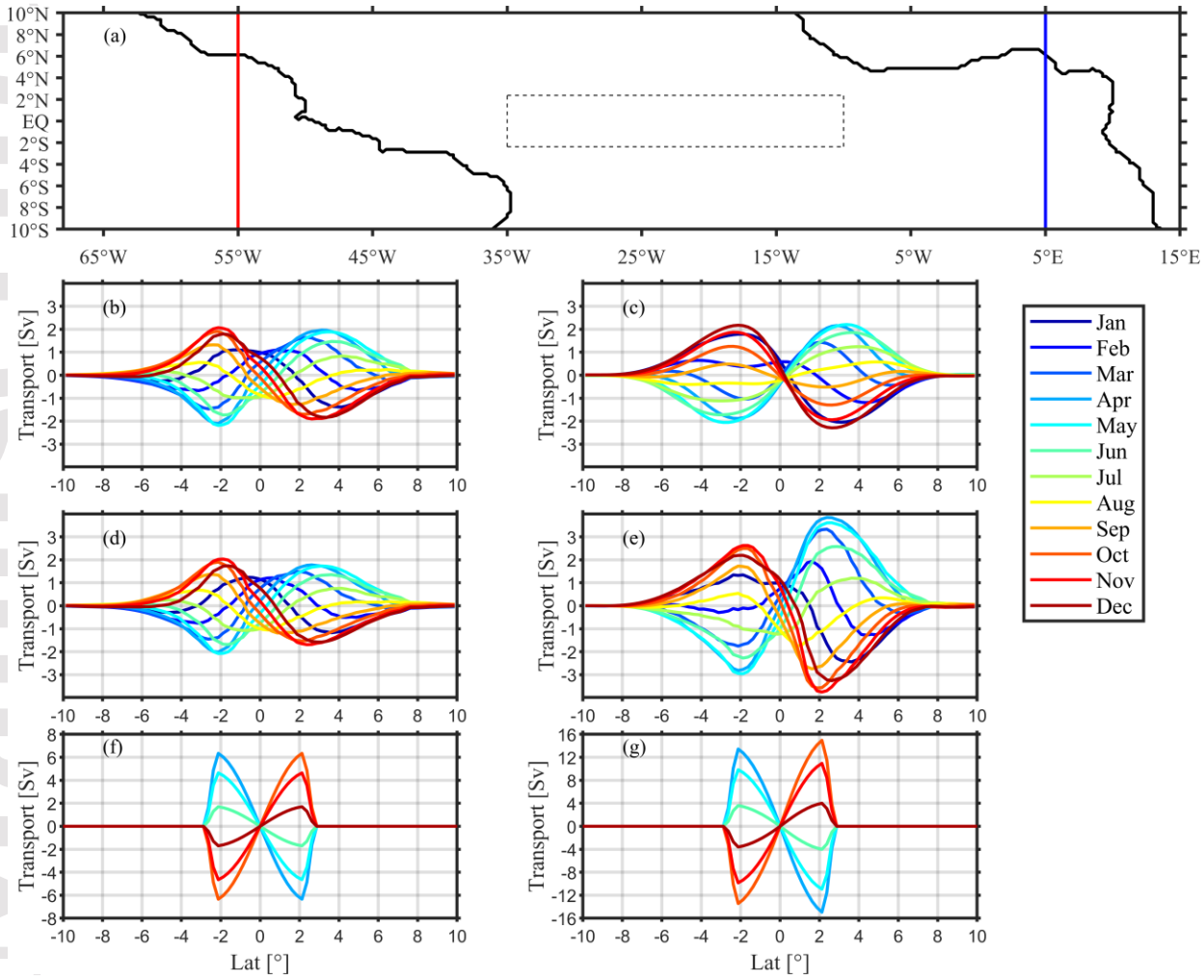

Figure 8. (a) The dashed-line box indicates the forcing area for E1-E3, red (blue) line replaces the western (eastern) boundary in E2 (E3); (b)-(e) The seasonal anomaly of the EWBC transport from E1-E4. In E4, the zonal wind stress is extended zonally to area from the western to the eastern boundary within 2.5°S-2.5°N range; (f) The seasonal anomaly of sverdrup transport calculated from the wind stress in E1; (g) same as (f) except for the wind stress in E4.

Experiment E2 uses the same wind forcing with E1, but replaces the western boundary with a straight line meridionally as shown by the red line in Figure 8a. Similarly, we conducted another experiment, E3, by replacing the eastern boundary with a straight line (indicated by the blue line in Figure 8a). Results from both E2 (Figure 8c) and E3 (Figure 8d) show clearly the

inter-hemispherical anti-symmetry in the seasonal anomaly of EWBC transport. The amplitude of variability, however, is similar on two sides of the equator in both experiments. The result supports our hypothesis that it's the equatorial forcing through symmetrical Rossby wave modes that is responsible for the anti-symmetric seasonal anomaly of the EWBC transport across the equator. It also indicates that the shape of either western or eastern boundary coastline is not a direct cause for the disparity of the seasonal transport amplitude on two sides of the equator. The changes of the coastlines in E2 and E3 do not affect the forcing in either experiment because the forcing region is sufficiently far away from two boundaries. We postulate that changes in the forcing areas due to slanted boundaries may have more profound impacts on the EWBC transports. We design additional E4 experiment in which the zonal wind stress, described in Eq. (5), is extended from the western to the eastern boundary. The amplitude of the transport anomaly is clearly enhanced in the northern hemisphere. This enhancement is due to the larger area of forcing because of the slanted western boundary. From Figure 7c, it is also clearly that the forcing area in the north equatorial Atlantic (between red dashed line and black dashed line) is lager that the south equatorial Atlantic (between blue dashed line and black dashed line). And, the forcing area difference is more related with the slanted western boundary rather than the eastern boundary. From Sverdrup balance, we can clearly know that under the homogeneous wind stress curl forcing, the larger ocean area will generate the stronger interior Sverdrup transport which will result in a corresponding stronger western boundary current (as the results shown in Figure 8f and 8g). The results from this set of idealized forcing experiments further support the conclusion from experiments M1-M5 using realistic forcing.

5 Summary

In this paper, we have examined the latitudinal differences of EWBC seasonal transport in tropical Atlantic Ocean. Two sets of data-assimilated simulations, ECCO4r3 and SODA3.4.2, are used for diagnoses of the EWBC seasonal variations. Our analyses of both ECCO4 and SODA products reveal two prominent features of the seasonal variability of the EWBC: (1) the seasonal change in the EWBC transport is anti-symmetric across the equator, and (2) the amplitude of transport variability is much greater in the northern hemisphere. The EWBC transport variability has seldom been studied as a whole system in previous studies which focused mostly on selected sections where observations were made. For example, Johns et al. (1998) used observations to show that the western boundary current was weak during April-June north of the equator. Our study is not only consistent with their finding but also links changes in EWBC to basin-scale adjustment processes, i.e., the generation and propagation of equatorial waves.

We find that the anti-symmetry of the EWBC transport in ECCO4 and SODA is mainly due to the impingement of odd-numbered meridional modes (symmetrical modes) of equatorial Rossby waves on the western boundary. This conclusion is supported by a series of simulations using a simple 1 and 1/2 layer model. Our control run is able to simulate the two key features that are identified in our analyses of ECCO4 and SODA. Several additional sensitivity tests are made to identify, isolate and examine forcing mechanisms. It is found that it's mainly the zonal wind stress along the equator that generate the symmetrical Rossby wave modes that remotely influences EWBC's seasonal variability. Anti-symmetrical Rossby waves, i.e., even-numbered meridional modes, play a relatively small role.

494 We have also designed another set of experiments to examine whether and how the
495 slanted coastlines affect the EWBC variability. In our 1 and 1/2 layer model the shape of the
496 coastline could have two effects. It affects the reflection of equatorial waves and also affects the
497 ocean area. Our experiments indicate that the first effect, i.e., the impact on the wave reflection,
498 is rather small. The main effect through the ocean-land contrast between the northwestern and
499 southwestern equatorial Atlantic Ocean. The northwestward slanted coastline along the western
500 boundary makes the EWBC subject to a larger area of equatorial wind-stress forcing than that in
501 the southern hemisphere. It is also found that the shape of coastline along the eastern boundary
502 has little impact on the EWBC variability.

503

504 **Acknowledgements**

505 Jiayan Yang is supported by the National Science Foundation, the WHOI-OUC
506 Collaborative Initiative and the W. V. A. Clark Chair for Excellence in Oceanography from
507 WHOI. Yujia Zhai is financially supported by China Scholarship Council to study at WHOI as a
508 two-years guest student. Yujia Zhai and Xiuquan Wan are supported by National Natural Science
509 Foundation of China major project (41776009). The ECCO4 products are freely available from
510 https://www.ecco-group.org/. The SODA3 products are freely available from
511 https://www2.atmos.umd.edu/~ocean/index.htm. We sincerely thank the two reviewers for their
512 constructive and thoughtful comments that have helped us improve our work.

513

514 **References**

515 [1] Amante, C.; Eakins, B.W. (2009), "ETOPO1 1 Arc-Minute Global Relief Model: Procedures,
516 Data Sources and Analysis". *NOAA Technical Memorandum NESDIS NGDC-*
517 *24*. doi:10.7289/V5C8276M.

[2] Bourlès, B., Gouriou, Y., and Chuchla, R. (1999), On the circulation in the upper layer of the western equatorial Atlantic, *J. Geophys. Res.*, 104(C9), 21151– 21170, doi:10.1029/1999JC900058.

[3] Bourles, B., Molinari, R. L., Johns, E., Wilson, W. D., and Leaman, K. D. (1999), Upper layer currents in the western tropical North Atlantic (1989–1991), *J. Geophys. Res.*, 104(C1), 1361– 1375, doi:10.1029/1998JC900025.

[4] Busalacchi, A. J., & Picaut, J. (1983), Seasonal Variability from a Model of the Tropical Atlantic Ocean, *J. Phys. Oceanogr.*, *13*(9), 1564-1588, doi: 10.1175/1520-0485(1983)013%3C1564:SVFAMO%3E2.0.CO;2

[5] Carton, J. A., Chepurin, G. A., and Chen, L. (2018), SODA3: A New Ocean Climate Reanalysis. *J. Climate*, 31, 6967–6983, doi:10.1175/JCLI-D-18-0149.1.

[6] Carton, J. A., Penny, S. G., and Kalnay, E. (2019), Temperature and Salinity Variability in the SODA3, ECCO4r3, and ORAS5 Ocean Reanalyses, 1993–2015. *J. Climate*, 32, 2277–2293, doi:10.1175/JCLI-D-18-0605.1.

[7] da Silveira, I. C. A., de Miranda, L. B., and Brown, W. S. (1994), On the origins of the North Brazil Current, *J. Geophys. Res.*, 99(C11), 22501– 22512, doi:10.1029/94JC01776.

[8] Dee, D.P., Uppala, S.M., Simmons, A.J., Berrisford, P., Poli, P., Kobayashi, S., et al. (2011), The ERA-Interim reanalysis: configuration and performance of the data assimilation system. *Q.J.R. Meteorol. Soc.*, 137, 553-597. doi:10.1002/qj.828.

[9] Forget, G., Campin, J.-M., Heimbach, P., Hill, C. N., Ponte, R. M., and Wunsch, C. (2015), ECCO version 4: an integrated framework for non-linear inverse modeling and global ocean state estimation, *GEOSCI MODEL DEV*, 8, 3071-3104, doi:10.5194/gmd-8-3071-2015.

[10] Fukumori, I., Wang, O., Fenty, I., Forget, G., Heimbach, P., and Ponte, R. M. (2017), ECCO Version 4 Release 3, http://hdl.handle.net/1721.1/110380, doi:1721.1/110380. Available at ftp://ecco.jpl.nasa.gov/Version4/Release3/doc/v4r3_estimation_synopsis.pdf.

[11] Gill, A.E. (1980), Some simple solutions for heat-induced tropical circulation. *Q.J.R. Meteorol. Soc.*, 106: 447-462, doi:10.1002/qj.49710644905.

[12] Hazeleger, W., de Vries, P., and Friocourt, Y. (2003), Sources of the Equatorial Undercurrent in the Atlantic in a High-Resolution Ocean Model, *J. Phys. Oceanogr.*, 33, 677–693, doi:10.1175/1520-0485(2003)33<677:SOTEUI>2.0.CO;2.

[13] Hummels, R., Brandt, P., Dengler, M., Fischer, J., Araujo, M., Veleda, D., and Durgadoo, J. V. (2015) Interannual to decadal changes in the western boundary circulation in the Atlantic at 11°S, *Geophys. Res. Lett.*, 42, 7615– 7622, doi:10.1002/2015GL065254.

[14] Johns, W. E., Lee, T. N., Beardsley, R. C., Candela, J., Limeburner, R., and Castro, B. (1998), Annual Cycle and Variability of the North Brazil Current, *J. Phys. Oceanogr.*, 28, 103–128, doi:10.1175/1520-0485(1998)028<0103:ACAVOT>2.0.CO;2.

[15] McCreary, J., Julian, P., Picaut, J., and Moore, D.W. (1984), Effects of remote annual forcing in the eastern tropical Atlantic Ocean, *J. Mar. Res.*, 42, 45-81(37), doi:10.1357/002224084788506167.

[16] McDougall, T.J. and P.M. Barker, 2011: Getting started with TEOS-10 and the Gibbs Seawater (GSW) Oceanographic Toolbox, 28pp., SCOR/IAPSO WG127, ISBN 978-0-646-55621-5.

[17] Peterson, R. G., and Stramma, L. (1991), Upper-level circulation in the South Atlantic Ocean, *Prog. in Oceanogr.*, 26(1), 1-73, doi:10.1016/0079-6611(91)90006-8.

[18] Philander, S. G. H., and Pacanowski, R. C. (1986), A model of the seasonal cycle in the tropical Atlantic Ocean, *J. Geophys. Res.*, 91(C12), 14192– 14206, doi:10.1029/JC091iC12p14192.

[19] Richardson, P. L., and Walsh, D. (1986), Mapping climatological seasonal variations of surface currents in the tropical Atlantic using ship drifts, *J. Geophys. Res.*, 91(C9), 10537–10550, doi:10.1029/JC091iC09p10537.

[20] Rühs, S., Getzlaff, K., Durgadoo, J. V., Biastoch, A., and Böning, C. W. (2015), On the suitability of North Brazil Current transport estimates for monitoring basin-scale AMOC changes, *Geophys. Res. Lett.*, 42, 8072– 8080, doi:10.1002/2015GL065695.

[21] Schott, F. A., Brandt, P., Hamann, M., Fischer, J., and Stramma, L. (2002), On the boundary flow off Brazil at 5–10°S and its connection to the interior tropical Atlantic, *Geophys. Res. Lett.*, 29(17), 1840, doi:10.1029/2002GL014786.

[22] Schott, F. A., Dengler, M., Zantopp, R., Stramma, L., Fischer, J., and Brandt, P. (2005), The Shallow and Deep Western Boundary Circulation of the South Atlantic at 5°–11°S, *J. Phys. Oceanogr.*, **35**, 2031–2053, doi:10.1175/JPO2813.1.

[23] Schott, F. A., Fischer, J., and Stramma, L. (1998), Transports and Pathways of the Upper-Layer Circulation in the Western Tropical Atlantic, *J. Phys. Oceanogr.*, 28, 1904–1928, doi:10.1175/1520-0485(1998)028<1904:TAPOTU>2.0.CO;2.

[24] Schott, F. A., Stramma, L., and Fischer, J. (1995), The warm water inflow into the western tropical Atlantic boundary regime, spring 1994, *J. Geophys. Res.*, 100(C12), 24745– 24760, doi:10.1029/95JC02803.

[25] Silva, M., Araujo, M., Servain, J., Penven, P., and Lentini, C. A.D. (2009), High-resolution regional ocean dynamics simulation in the southwestern tropical Atlantic, *Ocean Model*, 30(4), 256-269, doi:10.1016/j.ocemod.2009.07.002.

[26] Stramma L., Fischer, J., and Reppin, J. (1995), The North Brazil Undercurrent, *Deep-Sea Res.*, 42(5), 773-795, doi:10.1016/0967-0637(95)00014-W.

[27] Stramma L., and Schott, F. (1999), The mean flow field of the tropical Atlantic Ocean, *Deep-Sea Res.*, 46, 279-303, doi:10.1016/S0967-0645(98)00109-X.

[28] Weisberg, R. H., and Weingartner, T. J. (1988), Instability Waves in the Equatorial Atlantic Ocean, *J. Phys. Oceanogr.*, 18, 1641–1657, doi:10.1175/1520-0485(1988)018<1641:IWITEA>2.0.CO;2.

596 [29] Wienders, N., Arhan, M., and Mercier, H. (2000), Circulation at the western boundary of the
597 South and Equatorial Atlantic: Exchanges with the ocean interior, *J. Mar. Res.*, 58(6), 1007-
598 1039, doi:10.1357/002224000763485782

599 [30] Yang, J. (1999), A linkage between decadal climate variations in the Labrador Sea and the
600 tropical Atlantic Ocean, *Geophys. Res. Lett.*, 26, 1023–1026, doi: 10.1029/1999GL900181.

601 [31] Yang, J., and Joyce, T. M. (2006) Local and Equatorial Forcing of Seasonal Variations of
602 the North Equatorial Countercurrent in the Atlantic Ocean. *J. Phys. Oceanogr.*, 36, 238–
603 254, doi:10.1175/JPO2848.1.

604 [32] Yu, L., and Jin, X. (2010) Satellite-based global ocean vector wind analysis by the
605 Objectively Analyzed Air-sea Flux (OAFlux) Project: Estab- lishing consistent vector wind time
606 series from July 1987 onward through synergizing microwave radiometers and scatterometers,
607 Tech. Rep. OA-2010-01, WHOI OAFlux, Woods Hole Oceanographic Institution, Woods Hole,
608 Mass.

609 [33] Zhao, J. and Johns, W. (2014), Wind-Driven Seasonal cycle of the Atlantic Meridional
610 Overturning Circulation, *J. Phys. Oceanogr.*, 44(6), 1541-1562, doi: https://doi.org/10.1175/JPO-
611 D-13-0144.1.

612 [34] Zhang, D., Msadek, R., McPhaden, M. J., and Delworth, T. (2011), Multidecadal variability
613 of the North Brazil Current and its connection to the Atlantic meridional overturning
614 circulation, *J. Geophys. Res.*, 116, C04012, doi:10.1029/2010JC006812.

615